Borehole EM Monitoring at Aquistore

Final Report to the Carbon Capture Project (CCP)

Thomas M. Daley, J. Torquil Smith, John Henry Beyer
(all at Lawrence Berkeley National Laboratory)

and

Douglas LaBrecque (Multi-Phase Technologies, LLC)

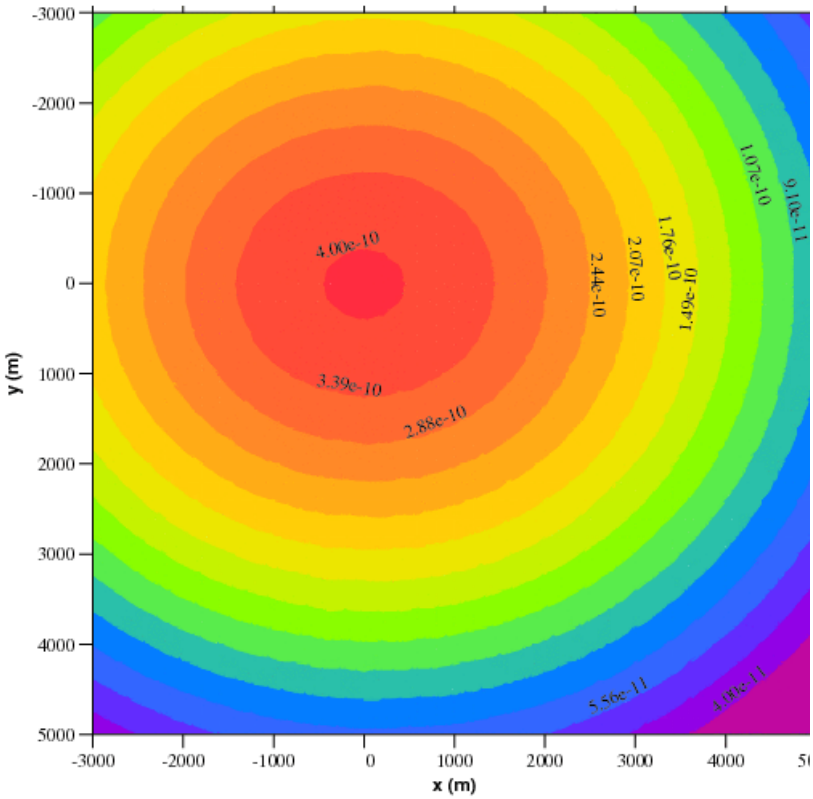

Table of Contents

Introduction **4**

Section I: Numerical Modeling of Borehole Source CSEM at Aquistore **5**

Background Resistivity Model Design 6

CO_2 Plume and EM Source Model 6

Modeling Results 7

Anomalous Surface Fields *8*

Surface Measurement S/N *9*

Response to Varying Injection Volumes *9*

Placement of Surface Sensor Stations *10*

Optimizing Source Location *11*

Use of Borehole Electrode Sensors in Single-Well Monitoring 12

Cable Crosstalk in Single-Well Monitoring *13*

Use of Borehole Magnetometers 15

Modeling Summary and Conclusions **15**

Section II: Design Engineering for Aquistore Borehole EM Monitoring **17**

Design Overview 17

Electrode Design 19

Cable Design 22

Design 1 ..... *23*

Design 2 ..... *25*

Engineering Design Conclusions/ Recommendations **26**

Appendix A Cable Heating **27**

The temperature increase near an electrode. *27*

Acknowledgements **29**

References **29**

List of Figures

Figure 1: 1-D resistivity model used in this study, taken from averaged resistivity analysis from Imperial Halkett Well 15 7 3 8. 7

Figure 2: Detail of vertical conductivity model on finite-difference gridding, with 10 kt CO_2 injected, showing wells and source dipole location. 7

Figure 3: Surface anomalous horizontal electric field (Eh) for 10 kt CO_2 with 360 amp-m, 1 Hz downhole source. 8

Figure 4: Surface anomalous horizontal magnetic field (B_h) for 10 kt CO_2 with 360 amp-m, 1 Hz downhole source. 8

Figure 5: Surface anomalous vertical 360 amp-m, 1 Hz downhole source. 9

Figure 6: Surface anomalous horizontal magnetic field (B_h) for 2.5 kt CO_2 with 360 amp-m, 1 Hz downhole source. 9

Figure 7: Surface anomalous horizontal magnetic (B_h) field for 250 kt CO_2 with 360 amp-m, 1 Hz downhole source. 10

Figure 8: Maximum changes in surface horizontal and vertical magnetic fields and in horizontal electric fields at Earth's surface, for 360 amp-m dipole at 1 Hz. 10

Figure 9: Mass (kt) of CO_2 needed for 4:1 signal to anticipated noise level in surface anomalous B_h, 360 amp-m, 1 H_z downhole source. 11

Figure 10: Mass (kt) of CO_2 needed for 4:1 signal to anticipated noise level in surface anomalous B_z 360 amp-m, 1 H_z downhole source. 11

Figure 11: Anomalous vertical electric fields (E_z) measured at the observation well, as a function of depth for various amounts of CO_2. 13

Figure 12: Relative anomalous vertical electric field (E_z) in observation well, as a function of depth for various amounts of CO_2. 13

Figure 13: Expected inductive crosstalk between the source electrode cable and downhole receiver electrode leads as a function of the separation between the source cable and receiver leads. 15

Figure 14: Anomalous horizontal magnetic field (By), as a function of depth, for various amounts of CO_2. 15

List of Tables

Table 1. Companies that can provide high power, high voltage and current controlled waveform transmitters 17

Table 2. The average resistivity from well log data in four wells near the Aquistore site. The resistivity values are given near the Precambrian bedrock 22

Table 3. Estimated Costs for the armored wire line cable (Design 1) 24

Table 4. Estimated Costs for the custom built cable (Design 2) 26

Introduction

Geologic carbon sequestration (GCS) is a technology whose goal is to prevent atmospheric release of greenhouse gases via injection of carbon dioxide (CO_2) into an underground reservoir for long term storage. GCS is typically part of a program of carbon capture and storage (CCS) that captures CO_2 from point sources such as power plants, transports the CO_2 to a storage site, and operates an injection facility. One recent CCS pilot project is the Aquistore CO_2 sequestration project, near Estevan, Saskatchewan, Canada. The Aquistore project is managed by the Petroleum Technology Research Centre (PTRC) and will be one of the first integrated CCS projects storing CO_2 in a deep saline aquifer from a coal fired power plant (PTRC, 2011). Aquistore is expected to store 500,000 tons of CO_2 during its lifetime (Ministry of Environment, 2012).

Assuring the long-term, safe storage of CO_2 requires the development of effective monitoring strategies. As part of the geophysical monitoring effort at Aquistore, there were initial plans for deployment of borehole electrodes for electrical or electromagnetic measurements to monitor CO_2 within the reservoir. The injected CO_2 displaces saline brine in the reservoir, and because CO_2 has a high resistivity compared to brine, the overall resistivity of the formation increases and can be monitored by measuring electric or magnetic fields. Previous work by Lawrence Berkeley National Laboratory (LBNL) had indicated that borehole-to-surface electromagnetic monitoring, using an electric dipole source near the bottom of a well penetrating the reservoir, could detect the resistivity change induced by GCS.

To assess the potential application of electromagnetic monitoring at Aquistore, Lawrence Berkeley National Laboratory and Multi-Phase Technologies collaborated on a two-part study including (1) numerical forward modeling of a time-lapse, controlled-source electromagnetic (CSEM) monitoring survey, and (2) an initial engineering study of instrumentation and proposed design for a borehole electric dipole source and electrode sensors.

This study addresses a specific geologic/geophysical model for the Aquistore site and the engineering design limitations imposed by the specific Aquistore monitoring well deployment. As such, this is a site-specific study and not a generic analysis. The modeling work was focused on determining the potential detection of injected CO_2 with a borehole electric dipole source and, as such, it was a forward-modeling detection study designed to guide the acquisition geometry and give a go/no-go decision point. We did not undertake a plume-mapping study, which would need to include an inversion with sensitivity analysis to understand resolution. However, we did look at estimated noise levels to assess likely detectability of the plume in field data for various plume sizes

This report summarizes the results of the study in two sections. In Section I, we will present the background model development, including CO_2 and CSEM source

properties. The model results, including response to varying injection volumes, are included in Section 1, along with a study of optimizing the source location within the borehole. Also included is a consideration of using borehole sensor electrodes (single-well measurement) with analysis of the effect of cable crosstalk for the proposed Aquistore deployment cables, as considered by the engineering study.

In Section II, we present an engineering design study specifically focused on the planned monitoring well for Aquistore. The engineering design section builds on the numerical results of the first section to consider the design of the electromagnetic (EM) transmitter and its ability to provide sufficient current, voltage, and power. The specific hardware considered is that which is best suited for the specific project constraints known at the time of the work, including factors such as borehole diameter, depth, time to completion, and delivery time of fabricated components. The hardware in the engineering design includes borehole electrodes for sources and sensors and the wire/cables which would run to surface.

Note that work on the two sections was carried out largely in parallel due to the short time available for possible deployment at Aquistore. Therefore, there are some differences, notably in the placement of the source electrodes (at the top of reservoir for modeling, below and above the reservoir for engineering).

Section I: Numerical Modeling of Borehole Source CSEM at Aquistore

Electromagnetic (EM) response to partial brine displacement by a resistive fluid has been modeled before. For example, Hoversten and Gasperikova (2006) report changes in modeled in-line surface electric fields due to the presence or absence of CO_2 on the order of 1.5% for injection of ~4 Mt (megatonnes) (~7×10^6 m^3 *in situ*) of CO_2 in sands at 1,100 m to 1,400 m depth, for a roving surface horizontal electric dipole source. Andréis and MacGregor (2010) found measurable seafloor electric field sensitivity to the withdrawal of 4×10^5 m^3 (~3×10^5 m^3 *in situ*) of natural gas from 1,100 m to 1,400 m below seafloor instruments. However, source fields typically fall off as $1/r^3$ away from a (low frequency) dipole source, and anomalous fields due to localized targets fall off as $1/r^3$ (e.g., dipole fields), or as $1/r^2$ (e.g., magnetic fields due to secondary currents of electric dipole moment of target), making imaging of localized zones at depths much over 2 km below sources and receivers fairly difficult. Thus, single-well, cross-well, or wellbore-to-surface measurements can be more sensitive to the injection or withdrawal of gas at large depths. For example, Swanepoel et al. (2012) show 2% to 100% anomalies in synthetic single-well electric field data 300 m from 0.1 to 10 kt (kilotonnes) CO_2 injected in a resistive layer in a homogeneous background.

Background Resistivity Model Design

Our simulated injection of CO_2 is into the lower Deadwood formation from 3,370 to 3,400 m, as is anticipated for the Aquistore Esteban CO_2 injection well. We assume a temperature of 107°C, consistent with well bottom temperatures in the area and a vertical geothermal gradient of 0.04°C/m. We assume 350 grams/liter (g/L) (350,000 ppm) salinity, consistent with values for the Deadwood formation at a similar depth in a plotted cross section of the Weyburn field slightly to the north of the Esteban drill site (from Whittacker, et al., 2009). This gives an estimated brine conductivity of 70 siemens/m (resistivity of 0.014 ohm-m) (at 100°C). To estimate *in situ* resistivity, we assume hydrostatic pressure and a porosity of 5%, and we use Archie's law with parameters a = 0.62 and m = 1.95, typical for well-cemented Paleozoic sediments, and well log resistivities from the nearby Imperial Halkett Well 15 7 3 8 (unique well number 101150700308W200_1524_MD_L1_MD) adjusted for differences between micro laterolog resistivities and long- and short-normal resistivities. For the depths injected with CO_2, we assume a gaseous (supercritical) saturation of 0.3, and a slight amount in aqueous solution (extrapolated from solubility values at 90°C, 300 bars and 0, 20, 50, 80, and 100 g/l salinity given in Doughty, 2009).

In the area around the Aquistore site, deep horizons dip less than 1% (see cross section in Whittacker et al., 2009), so we use a one-dimensional (1-D) resistivity model. We average well log resistivities from the Imperial Halkett well into a 1-D anisotropic model with vertical and horizontal resistivities given by series and parallel averages of the well log resistivities. Boundaries between layers were selected sequentially at the maxima of a Komolgorov-Smirnov statistic (e.g., Press et al., 1986) on the distribution of well log resistivities normalized by layer mean resistivities. The number of layers were kept to 15 (plus a basement half-space), which models the gross variation in well log resistivities with depth, while retaining an overall simplicity. Where available, 1.5 times the long-normal resistivity less 0.5 times the short-normal resistivity was used to represent the formation resistivity. In the lower parts of the well, only micro laterolog values were available, which, in the upper part of the well, were consistently higher than short- and long-normal resistivities, so they were scaled using scale factors estimated from higher in the well. Resistivity values for the Prairie evaporate formation (salt) were replaced with a 100 ohm-m value, because while salt-saline surfaces at a well are conductive, salt in bulk is resistive. The depths of the model resistivity layers were increased slightly to put the Precambrian basement at 3,400 m, anticipated at the Esteban drill site. Based on a comparison of basement resistivities from other wells in the area, the measured 90 ohm-m basement resistivity was replaced with a 400 ohm-m value. The resistivity model resulting from the above analysis is shown in Figure 1.

CO_2 Plume and EM Source Model

For the study, CO_2 was modeled as injected into a 30 m thick reservoir layer from 3,370 to 3,400 m depth. Within the background resistivity model, the reservoir layer is not distinguished from layers above it, as the Komolgorov-Smirnov statistic at its

top is smaller than at the boundaries of the 15 layer model. The injected CO_2 is modeled as a 30 m high inverted (upside down) spherical cap of the requisite volume, centered laterally at the injection well. The injection well is 100 m from the observation well in the x direction. A down-hole vertical electric dipole source was modeled at the top of the reservoir layer in the observation well, as shown in Figure 2. Based on the well logs, an 8.6 ohm-m average resistivity is anticipated in the reservoir before CO_2 injection, and this value was used for calculating the anticipated dipole current available. In this dipole, two electrodes 2 m long x 0.2 m diameter are separated 30 m and have 4.1 ohms contact resistance. Connecting each to four 3,400 m long #20 (amer.) gauge wires in parallel adds 65.2 ohms. Against 69.3 ohms, a 10 kW source produces 12.0 amperes at 832 V, yielding a source dipole moment of 360 amp-m. A configuration with the source dipole at the top of the injection horizon enables inducing some horizontal electric fields in the CO_2, and assures good electric contact with the injection horizon. A detail of the source dipole and CO_2 injection configuration is shown in Figure 2, together with model vertical conductivity values after discretization on the finite difference grid used in modeling, for the case of 10 kt injected CO_2.

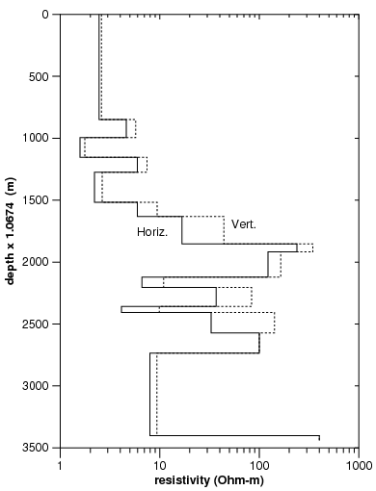

Figure 1: 1-D resistivity model used in this study, taken from averaged resistivity analysis from Imperial Halkett Well 15 7 3 8.

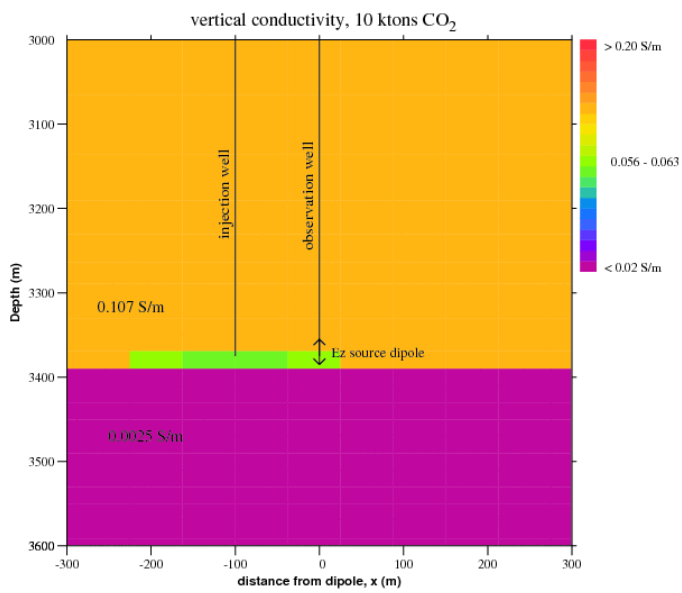

Figure 2: Detail of vertical conductivity model on finite-difference gridding, with 10 kt CO_2 injected, showing wells and source dipole location.

Modeling Results

We model fields between ±15,840 m in x and y, and from -14,321 to 14,066 m in z (down) using the code of Commer and Newman (2008) in a forward modeling mode using a secondary field formulation with primary fields determined by the 1-D

model section at the injection well prior to injection. The fields were modeled on a 105 by 105 by 73 grid, with 250 m grid spacing in x and y over most of the central ±6,115 m, decreasing to 62.5 m near the well, with 20 m vertical spacing in the 260 m surrounding the injection zone, increasing to 300 m spacing by 1,265 to 1,865 m depth, and decreasing to 193 m vertical spacing near the Earth's surface.

Anomalous Surface Fields

To view the effect of CO_2 injection, we calculate the anomalous fields, i.e., the difference in a given EM field component between the model with CO_2 injected and the baseline model (no CO_2). Anomalous horizontal electric, horizontal magnetic, and vertical magnetic field magnitudes (at 1 Hz) at the Earth's surface are shown in Figures 3-5, respectively, for the case of 10 kt injected CO_2, scaled for a 360 amp-m source. These fields resemble those of a horizontal electric dipole at depth aligned in the direction of offset from injection well to transmitter dipole (x-direction in Figures 3-6). Such a dipole has magnetic field lines in rings about the dipole axis, and electric field lines emanating from one pole and returning to the other. This resemblance is consistent with the fields from a horizontal electric dipole moment induced in the CO_2 being reinforced by an image horizontal electric dipole in the resistive basement, because a no-current flow boundary condition holds approximately there, with fields from any similarly induced vertical electric dipole moment being effectively cancelled by its image in the basement which opposes it.

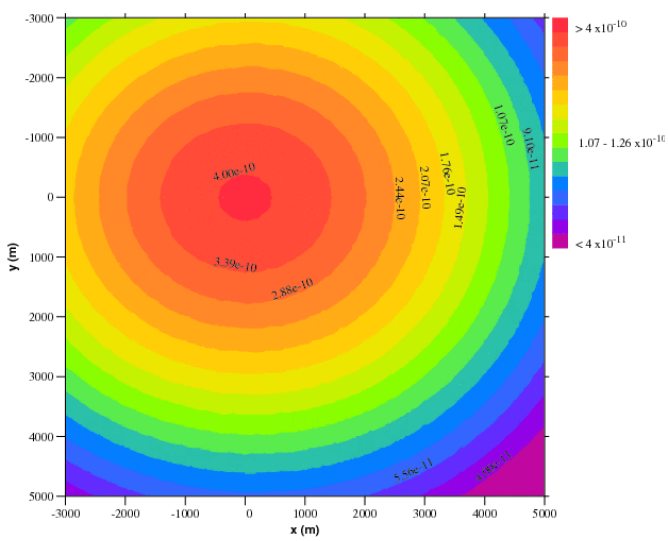

Figure 3: Surface anomalous horizontal electric field (Eh) for 10 kt CO_2 with 360 amp-m, 1 Hz downhole source.

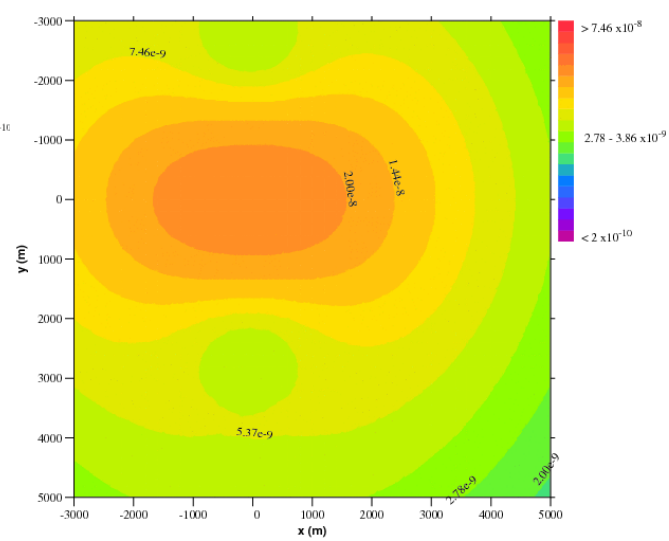

Figure 4: Surface anomalous horizontal magnetic field (B_h) for 10 kt CO_2 with 360 amp-m, 1 Hz downhole source.

In general, the use of a downhole vertical electric dipole source is important for producing vertical electric fields (the current flow direction) in the vicinity of a flat-lying resistive CO_2 plume, which results in significant anomalous electric and magnetic fields. However, the existence at the Aquistore site of a highly resistive basement immediately below the CO_2 reservoir and the source dipole significantly

reduces the anomalous fields. This highlights the importance of site-specific geologic conditions and the use of modeling to assess appropriate survey designs for CSEM monitoring.

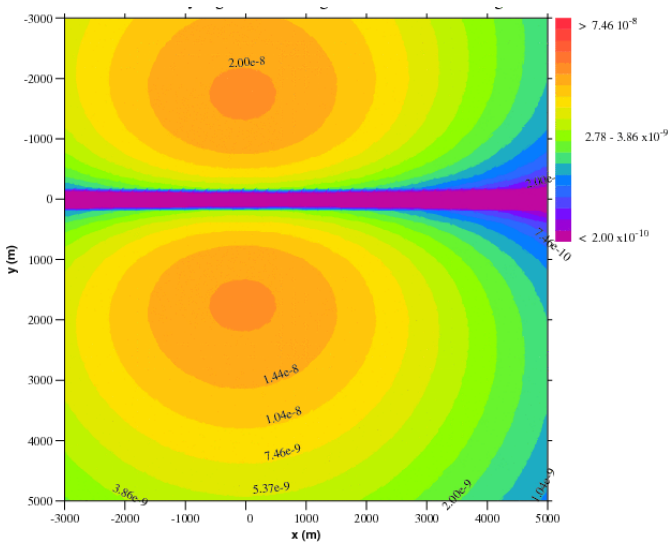

Figure 5: Surface anomalous vertical 360 amp-m, 1 Hz downhole source.

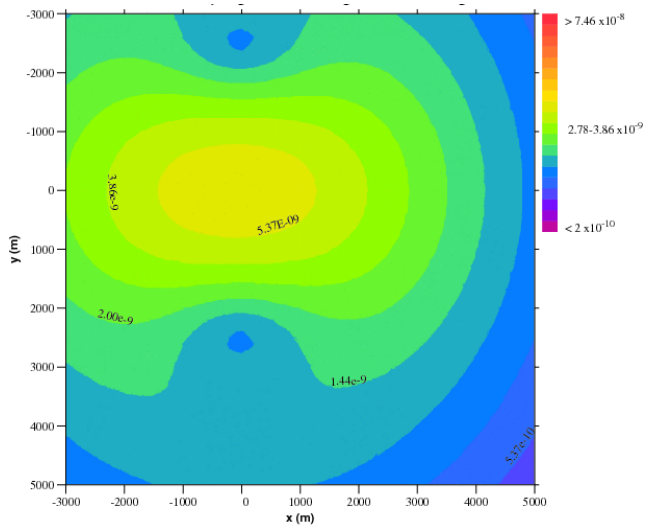

Figure 6: Surface anomalous horizontal magnetic field (B_h) for 2.5 kt CO_2 with 360 amp-m, 1 Hz downhole source.

Surface Measurement S/N

With 30 minutes of stacking (a reasonable acquisition time for each surface sensor site), anticipated noise levels at 1 Hz are 2.8×10^{-10} V/m in E_h, with copper-copper sulfate electrodes and 100-m electrode lines (based on electrode noise measurements by Petiau and Dupis, 1980), and 2×10^{-10} T (tesla) in B_h (assuming 95% cancellation of natural signals using a remote reference). Thus, for a 360 amp-m source and 10 kt CO_2, the maximum electric field anomaly rises a factor of 1.4 above electrode noise, whereas magnetic field anomalies attain signal-to-noise levels of 135 and 105 in B_h and B_z, respectively.

Response to Varying Injection Volumes

Surface anomalous E_h and B_h fields for 1 kt to 20 kt CO_2 and B_z fields for 1 kt to 1 Mt CO_2 are very similar in form to the 10 kt fields, while differing in amplitude. For example, surface anomalous B_h fields for 2.5 kt of CO_2 are shown in Figure 6. These are above the anticipated noise level throughout the plotted region. From 50 kt to 250 kt, surface anomalous B_h field shape changes continuously towards the fields at 250 kt shown in Figure 7 (with a different color scale). These are similar in form to the sum of fields from opposing horizontal electric dipoles induced on the CO_2 on either side of the source, with greater moment in the +x direction (away from the injection well). While difficult to measure, for more than 250 kt, the surface anomalous B_h field shape continues to change, towards fields with magnitudes which are symmetric on reflection about the observation well in both x and y directions (not shown).

For a 360 amp-m source dipole at 1 Hz, Figure 8 shows the maximum changes in horizontal and vertical magnetic fields and in horizontal electric fields at the Earth's surface as a function of the mass of CO_2 injected. The maximum anomalies are observed for 10 kt injected CO_2 (272 m horizontal span at top), with magnitudes 4×10^{-10} V/m (E_h), 2.7×10^{-8} T (B_h), and 2.1×10^{-8} T (B_z). Thus, maximum magnetic field anomalies are expected to rise above the noise level with injection of about 0.8 kt of CO_2, increase to a maximum at about 10 kt, and decrease to noise levels by 170 kt (for B_z) and by 270 kt (for B_h) corresponding to spherical caps with 710 and 770 m horizontal spans. Thus, the proposed experiment design can detect and monitor initial CO_2 injection with magnetic field anomalies, but may lose sensitivity for the planned 500,000-ton injection.

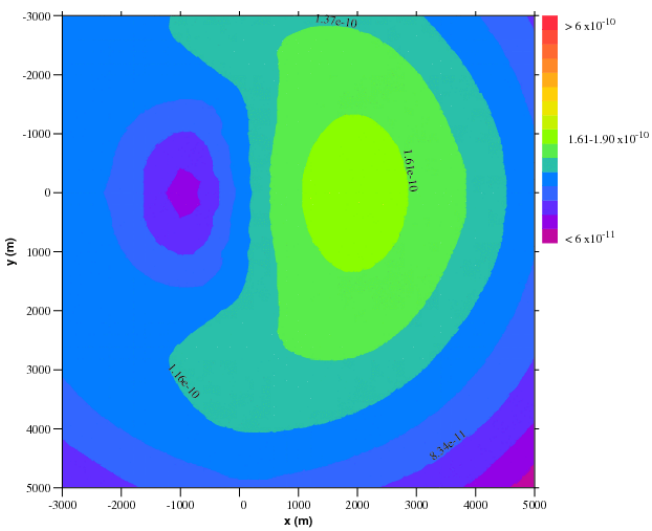

Figure 7: Surface anomalous horizontal magnetic (B_h) field for 250 kt CO_2 with 360 amp-m, 1 Hz downhole source.

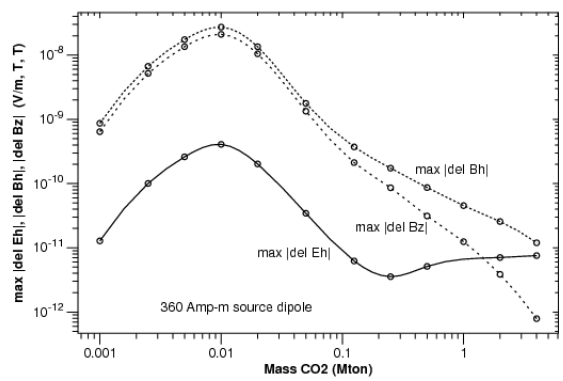

Figure 8: Maximum changes in surface horizontal and vertical magnetic fields and in horizontal electric fields at Earth's surface, for 360 amp-m dipole at 1 Hz.

Placement of Surface Sensor Stations

Regarding instrument location for sensitivity to various masses of injected CO_2 (i.e., survey area for monitoring CO_2 injection), we consider at what injection mass the anomalous field magnitudes are some multiple of the anticipated noise level. Figure 9 shows the mass of CO_2 needed for a 4:1 signal to anticipated noise level in a surface anomalous horizontal magnetic field. This shows B_h sensitivity to 1 kt of CO_2 only above the source transmitter location, with sensitivity to larger masses of CO_2 at greater distance from the source well location. Figure 10 is a similar plot for B_z sensitivity to CO_2 mass. Beyond about 7 km radius from the source well, the anomalous B_z magnitude drops below a 4:1 signal to anticipated noise ratio for all injected CO_2 masses modeled, whereas anomalous B_h does not fall below this ratio until a distance of 8.5 km from the source well.

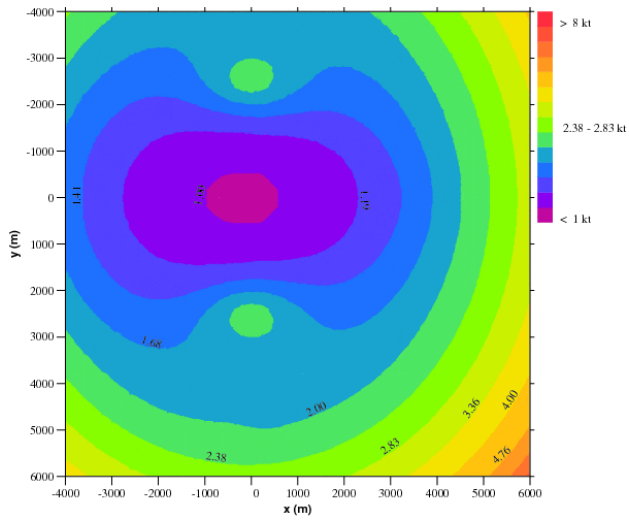

Figure 9: Mass (kt) of CO_2 needed for 4:1 signal to anticipated noise level in surface anomalous B_h, 360 amp-m, 1 H_z downhole source.

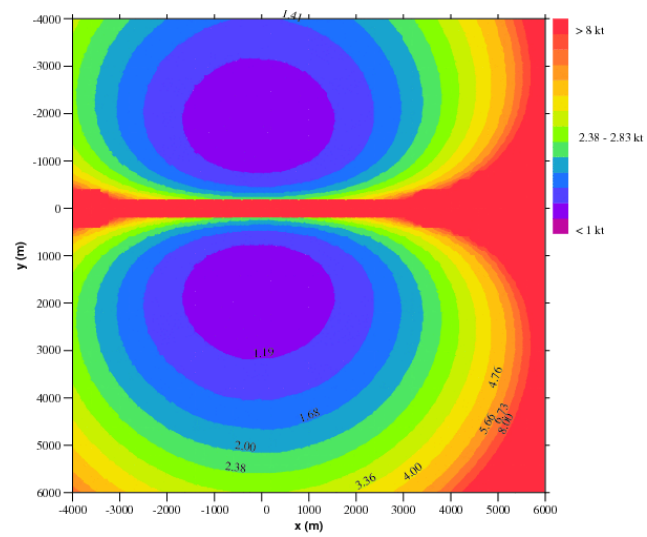

Figure 10: Mass (kt) of CO_2 needed for 4:1 signal to anticipated noise level in surface anomalous B_z 360 amp-m, 1 H_z downhole source.

Optimizing Source Location

The above results have been computed for a point dipole source at the top of the reservoir in which the CO_2 is injected (i.e., at top of inverted spherical cap of CO_2). Because the CO_2 plume is just above a resistive basement, surface measurements are mostly sensitive to the horizontal electric-dipole moments induced in the CO_2. This suggests using a vertical electric-dipole source centered a height of half the lateral offset to the CO_2 center, above the CO_2 center (e.g., 50 m above the CO_2 center) to maximize the horizontal electric field at the plume center. For the smallest CO_2 masses, that would double the signal levels above those reported here. Or, taking into account that the actual source is a finite length dipole rather than a point dipole, the electrode placement can be optimized to maximize the horizontal electric field at the plume center. In the zero frequency limit, for an electrode at distance x' laterally and height z_0' above the plume center, which itself is a height b above the resistive basement, and approximating the structure above basement as a uniform half-space, the horizontal electric field at the plume center is proportional to

$$E_h \propto \frac{x'}{(x'^2+z_0'^2)^{3/2}} + \frac{x'}{(x'^2+(z_0'+2b)^2)^{3/2}} \quad , \tag{1}$$

including effects of an image in the resistive basement. Assuming $|z_0'| \ll |x'|$, the horizontal electric field at the plume center is maximized for the electrode at

$$z_0' \approx \frac{-2b}{1+(1+4b^2/x'^2)^{5/2}} \tag{2}$$

for b = 15 m and x' = 100 m, z_0' = -13.4 m, suggesting a lower electrode 1.6 m above basement. Adding a second electrode at z_1' the horizontal electric field at the plume center is proportional to

$$E_h^{(t)} \propto \frac{x'}{(x'^2+z_0'^2)^{3/2}} - \frac{x'}{(x'^2+z_1'^2)^{3/2}} + \frac{x'}{(x'^2+(z_0'+2b)^2)^{3/2}} - \frac{x'}{(x'^2+(z_1'+2b)^2)^{3/2}} \quad (3)$$

Directly above the electrodes at the height of the Earth's surface the (zero frequency) horizontal magnetic field is proportional to

$$B_h^{(surf)} \propto \frac{1}{d-z_1'} - \frac{1}{d-z_0'} \ , \quad (4)$$

where d is the distance of the plume center below the Earth's surface. Using z_0 from Eq. (2) and using Eqs. (3-4), we maximize the ratio of $|E_h^{(t)}/B_h^{(surf)}|$ by searching the interval $[z_0', d]$ in small steps for the value z_1 giving its largest value. For the same values of b, x' and z_0', we have z_1' = 72.4 m, suggesting placing the upper source electrode 87.4 m above basement. Such an electrode configuration (1.6 m and 87.4 m above basement) would increase the horizontal electric fields at the plume center by a factor of 3.1 over those due to the point dipole considered above, so for the smallest CO_2 masses considered, the measured anomalous fields at the surface should increase by this factor.

Use of Borehole Electrode Sensors in Single-Well Monitoring

Since Aquistore was considering borehole electrodes in the same well as a possible borehole dipole source, it is interesting to think of the potential single-well measurements for monitoring. For the single well geometry, we have considered the sensitivity of downhole measurements of vertical electric field strengths as a function of depth and mass of injected CO_2. Figure 11 shows anomalous vertical electric fields in the observation well plotted as a function of depth below surface (at 25 m intervals) at 1 Hz, for the 360 amp-m vertical electric dipole source at 3370 m depth (as before), for 1, 2.5, 5, and 10 kt of injected CO_2. Amplitude increases and spikes at the source dipole depth as CO_2 mass approach 10 kt. (For actual finite length receiver electrode arrays, the measured signals are the receiver electrode separation times the field strengths plotted in Figure 11.) For the smallest CO_2 mass considered (1 kt, 79 m span), anomalous E_z evidently changes sign within the plotted interval, but not for the greater CO_2 masses considered.

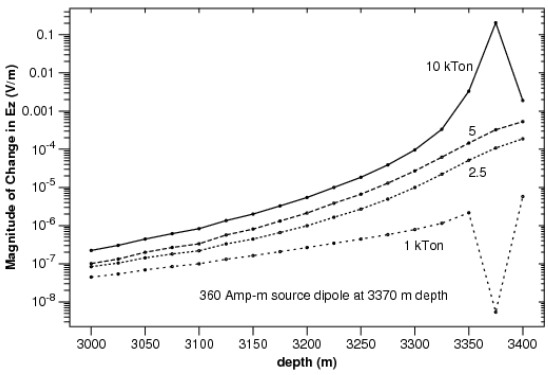

Figure 11: Anomalous vertical electric fields (E_z) measured at the observation well, as a function of depth for various amounts of CO_2.

Anomalous vertical electric field magnitudes, relative to vertical electric fields without the injected CO_2, are plotted in Figure 12. We see increased relative strength of the anomalous vertical electric field away from the source dipole where source fields are weaker, with maximum relative anomalies of 0.014, 0.027, 0.04 and 0.12 for 1, 2.5, 5, and 10 kt CO_2, respectively. These anomalous fields are much smaller than the previously mentioned results of Swanepoel et al. (2012), presumably due to the destructive interference of image dipole fields in the resistive basement immediately below the CO_2 mass (as discussed above).

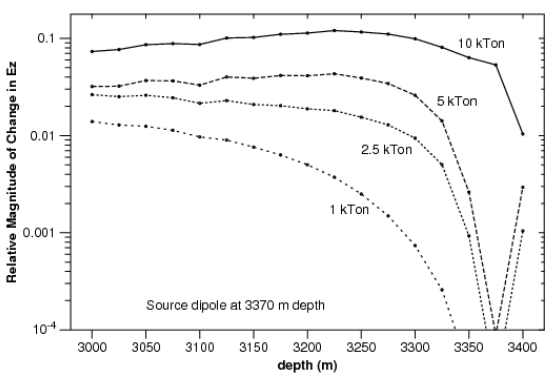

Figure 12: Relative anomalous vertical electric field (E_z) in observation well, as a function of depth for various amounts of CO_2.

Cable Crosstalk in Single-Well Monitoring

When using a monitoring well for a downhole dipole source and downhole magnetic and/or electric field sensors, an important issue is potential crosstalk between the cables going to the source and receivers. For the Aquistore monitoring well, there were constraints on the cables that could be deployed to carry current to the source electrodes. We therefore considered the effects of non-optimal cable design on the electrical crosstalk between source and receiver wires. A 12-conductor cable was

considered for powering the source electrodes (see Cable Design 1 in Section II below). The source cable design contained a set of three conductors 0.0029 m from the cable center and 120° from each other, connected to one electrode; and a similar set of three conductors rotated 40° from the first set, connected to the other electrode. A second 12-conductor cable with conductors separated by 0.00185 m would be used for leads to the receiver electrodes. The two cables were proposed to be deployed outside the well casing on opposite sides.

For comparison with the above single-well anomalous fields, Figure 13 plots the expected level of inductive crosstalk at 1 Hz between source dipole cables and downhole receiver dipole leads in a separate cable as a function of receiver lead/transmitter cable separation, for parallel transmitter and receiver cables and a 12 amp source dipole current. Since each of the cables consist of several wires, the relative positions of wires in one cable vary with respect to those in the other with rotation of either cable about its entire length. Therefore, inductive crosstalk depends on the rotation of each of the cables with respect to the other. The two inductive crosstalk values plotted are for the pair of cable rotations giving the largest magnitude crosstalk, and for the crosstalk averaged over all possible cable rotations. This assumes no twisting of cables, or identical twisting of source and receiver cables. Differing twists in source and receiver cables would give less inductive crosstalk. With some differences in twist randomizing orientations along the cables, the actual crosstalk is expected to be closer to the averaged crosstalk than to the worst case. For these cable configurations, crosstalk varies approximately inversely with the cube of the cable separation (and varies proportionally with frequency). A typical casing size for monitoring wells is 5.5 or 7 inches (14 or 18 cm) outer diameter, giving the maximum cable separation.

For a 1 cm separation between source cables and receiver leads, the expected inductive crosstalk at 1 Hz is 4×10^{-5} V; for 15 cm separation it is 9×10^{-8} V. The electrode noise levels expected at 1 Hz with half an hour of stacking is 4×10^{-8} V (with steel or brass electrodes). The magnitudes of average crosstalk noise and electrode noise are comparable at 21 cm cable separation, which is greater than the likely casing diameter. For 1 cm cable separation, crosstalk is much larger than electrode noise. So, for 1 cm receiver/transmitter cable separation (i.e., cables next to each other), with 10 m receiver electrode pair separation, for 1 kt injected CO_2, the magnitudes of all but one of the sample points of change in E_z plotted in Figure 11 are below that of the expected inductive crosstalk. For 2.5 kt injected CO_2, downhole E_z anomalies are above crosstalk in the bottom 125 m plotted. For 15 cm receiver/transmitter cable separation (e.g., for casing deployed cables), expected inductive crosstalk is below the E_z anomaly expected in the observation well due to CO_2 injections from 1 kt to 10 kt, for receiver electrodes spaced 3 m or more, for all but one of the points plotted in Figure 11. Thus, we see that crosstalk and cable separation are important variables to consider over the possible range of cable separations.

Use of Borehole Magnetometers

We have also computed downhole magnetic field responses. For a 1-D background conductivity, with the injection/observation well separation in the x-axis direction and a vertical electric dipole source in the observation well (as we have been considering), the only magnetic fields at the observation well are due to the inhomogeneity (the CO_2) and are in the y direction. Anomalous horizontal (By) responses at 1 Hz, for the same 360 amp-m vertical electric dipole source, for 1, 2.5, 5, and 10 kt of injected CO_2 are shown in Figure 14. Using simple 1000-turn 0.075 × 0.75 m (air core) windings as inductive sensors gives 56.25 m^2 effective coil area, and coil outputs of 56.25 V/T, so the lowest signal levels of Figure 14, would correspond to 2.3×10^{-5}, 2.8×10^{-4}, 8×10^{-4} and 1.3×10^{-3} V, respectively, for the four curves. For coils with no downhole amplification, crosstalk between transmitter cable and receiver cable is expected to be by far the largest source of noise. Assuming 10–15 cm transmitter/receiver cable separation, these signal levels are well above the expected crosstalk. Therefore, a borehole magnetic field sensor, possibly wireline deployed, is a feasible monitoring tool.

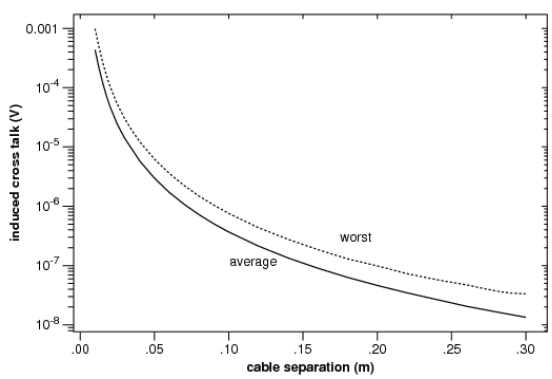

Figure 13: Expected inductive crosstalk between the source electrode cable and downhole receiver electrode leads as a function of the separation between the source cable and receiver leads.

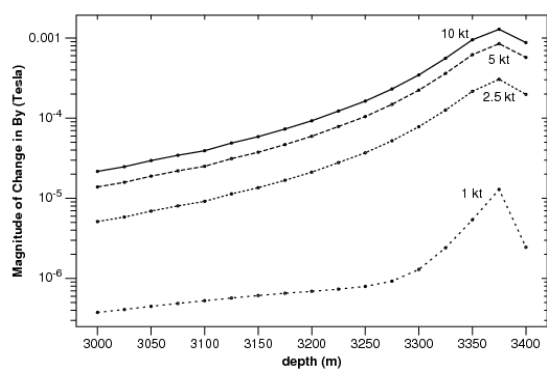

Figure 14: Anomalous horizontal magnetic field (By), as a function of depth, for various amounts of CO_2.

Modeling Summary and Conclusions

We have built a 1-D resistivity model of the Aquistore sequestration site. For this model, we have considered borehole-to-surface and single-well (i.e., borehole to shallower E-field measurements in the same well) EM monitoring using a downhole vertical electric dipole source. We have modeled a source with realizable moments, located in a monitoring well 100 m from the injection well, similar to the Aquistore site. The borehole-to-surface measurements are sensitive to injected CO_2 masses between 0.8 kt and 270 kt, with peak sensitivity at 10 kt. Downhole vertical electric

field measurements (the single-well configuration) are similarly sensitive to injected CO_2, but require separation of source and receiver cables for signals to rise above the expected crosstalk level induced in the sensor cable. Crosstalk is a function of cable design and location. We considered non-optimal cables due to specific project limitations and found the single-well CSEM method could still provide CO_2 detectability with adequate cable separation (e.g., 7 cm for 1 kt CO_2, 100 m well separation, and untwisted cables at 1 Hz).

An important conclusion is that the sensitivity of CSEM measurement is site specific. For the Aquistore geologic model of CO_2 injection just above resistive basement, the basement has a strong effect on the modeled EM fields. Also, there is a clear peak in sensitivity versus volume of injected CO_2, a result which again is specific to the site and transmitter/receiver geometry. We have shown that for a given model and well spacing, we can find an optimal source electrode location within the proposed EM source well.

The overall conclusion of this study is that the CSEM method with borehole source dipoles could be a useful monitoring tool for the planned Aquistore sequestration pilot.

Section II: Design Engineering for Aquistore Borehole EM Monitoring

Design Overview

This section discusses the design of the electromagnetic (EM) transmitter for a borehole dipole source and its ability to provide sufficient current, voltage, and power as described in Section I. There are several constraints to be considered when designing the EM transmitter. The constraints and design options to overcome the constraints are also discussed. Major design constraints include: (1) the total cable length of 3,400 m (including drilling 50 m into the basement) (2) instrumentation of the bottom 200 m of the borehole, and (3) the maximum transmitted (Tx) voltage of 1,000 volts. There are three major elements to the system design:

1) The surface transmitter that provides a carefully controlled current source,
2) The subsurface electrodes and supporting casing, and
3) Wires and cables to connect the electrodes to the subsurface.

Our suggestion is to make use of an existing, off-the-shelf, transmitter. The transmitter needs to provide high power, high voltage, and a current-controlled waveform with an accurate phase reference that can be used with one or more phase-locked receivers on the surface. Table 1 lists three possible transmitters. All three companies have significant track records in supplying this instrumentation. Two of the transmitters, the TXU-30 and the GGT-30, have almost identical specifications, including a maximum voltage of 1,000 volts and a maximum transmitted power of 30 kW. The third system, the IRIS VIP10000 has a much higher maximum voltage, 3,000 volts, but much lower maximum power, 10 kW.

Table 1. Companies that can provide high power, high voltage and current controlled waveform transmitters

Transmitter	Maximum Power	Maximum Voltage	Maximum Current
Iris Instruments VIP 10000	10 Kw	3,000 volts	20 amps
Phoenix Geophysics	30 Kw	1,000 volts	45 amps
Zonge Engineering	30 Kw	1,000 volts	45 amps

The design for the Aquistore monitoring well, at the time of our planning, called for the deployment of transmitting electrodes on the outside of the casing. A critical part of the design is to make certain that there are no conductive electrical pathways near the electrodes. Possible electrical pathways include:

1) The casing itself;
2) Tubing inside the casing;
3) Armored electrical cable;
4) Metal tubing along the outside of the casing for fiber-optic lines, electrical cables, fluid sampling, or other purposes; and
5) Electrical instrument housings with a common ground.

If any of these pathways come in direct, electrical contact with an electrode or multiple electrodes, they can completely short circuit the source dipole or provide a current path from one electrode to shallower depths. Either of these cases would decrease the effectiveness of the source dipole and/or create interference effects.

Even if the pathways discussed above do not directly contact the electrodes, they can still create significant effects if they are in electrical contact with the formation near the electrodes. To minimize these effects, it is important whenever possible to:

1) Use electrically nonconductive materials such a fiberglass for casings;
2) Use polymer encapsulated tubing for instrumentation;
3) Insulate housings of instruments with polymer resins; and
4) Isolate the grounds of down-hole instruments.

When it is not possible to completely insulate all of the metal surfaces from the formation, it is important to:

1) Keep the exposed metal surface as far from the electrode as possible; the impact of such a leakage path generally will decrease dramatically with increased distance;
2) Keep the exposed metal surface as small as possible, thus increasing its effective contact resistance; and
3) Avoid having dissimilar metals in contact with each other and the formation.

It is important to note that leakage effects are difficult to quantify and model. The surface impedance of the metal depends on the geometry of the surfaces, the types of metals, and the composition of the pore waters or cement in contact with the metal. It is strongly recommended that the electrodes are placed on fiberglass casing. Electrodes have been successfully deployed on fiberglass wrapped casing (Tøndel et al, 2011, Schmidt-Hattenburber et al, 2011) of well sites in the 800 to 1,000 m range. The site at Ketzin Germany (Schmidt-Hattenburger, et al, 2011) used Ryt-Wrap™, and the site described by Tøndel et al (2011) used a proprietary method. We are not aware of any deployments to depths of 3,000 m using fiberglass-wrapped casing. The primary issue with fiberglass-wrapped steel casing is the damage that can occur at the collars when making up the casing string and presence of centralizers and cable and instrument protectors.

Standard oil-field tooling invariably damages the fiberglass coating near the collars. The methods of dealing with this problem, ranked from the most to least practical, are:

1) Keep the electrodes as far from the damaged areas as possible by placing them near the mid joints.
2) Patch the damaged areas by painting them with quick-set epoxy or similar polymer. This is not difficult to do, but the value of the coating is questionable, particularly if it is applied in cold or wet conditions.
3) Place rubber sheeting or prefabricated covers over the joints. Often this is not compatible with other design aspects, such as centralizers and cable protectors.
4) Develop tooling that will not damage the fiberglass coatings. This is likely beyond the scope of this project.

Although there are a number of designs for casing centralizers and cable protectors used to secure the centralizers to the casing, the design invariably involves either set screws or metal teeth designed to bite into the metal casing. This pierces the electrically insulated fiberglass layer, and the entire surface of the centralizer/protector becomes a leakage path. There are a couple of work-arounds for this problem. The first work-around is to keep the electrodes as far from the centralizer/protector as possible. If the centralizers/protectors can be kept near the collars, then this work-around becomes feasible. The second work-around would be to use centralizers that do not pierce the fiberglass insulation. These types of centralizers were successfully implemented in the Ketzin study. Their centralizers used large, flat clamping surfaces, so the total static frictional force was sufficient to counteract the expected shear forces on the centralizers.

Electrode Design

Figure 15 shows the conceptual design for a 40-inch (roughly 1 m) long electrode used for monitoring of electric fields. The electrode was designed assuming a fiberglass-wrapped steel casing, but could easily be adapted to a fiberglass casing. Primary design considerations for the electrodes are to provide effective electrical insulation between the steel casing and the electrode, and make certain the electrode does not move on the casing during well completion. The proposed design uses a pair of half-cylinder shells of stainless steel (type 316) that are bolted together. The inside of the electrode is covered with a layer of fiberglass to provide an additional layer of insulation and is attached from the coated metal casing using a circular metal block that is welded to the casing. The metal block is covered with a layer of fiberglass, then covered by a cup-shaped cap of PEEK or similar plastic. The electrode is designed to fit over the metal block locking it into place on the casing.

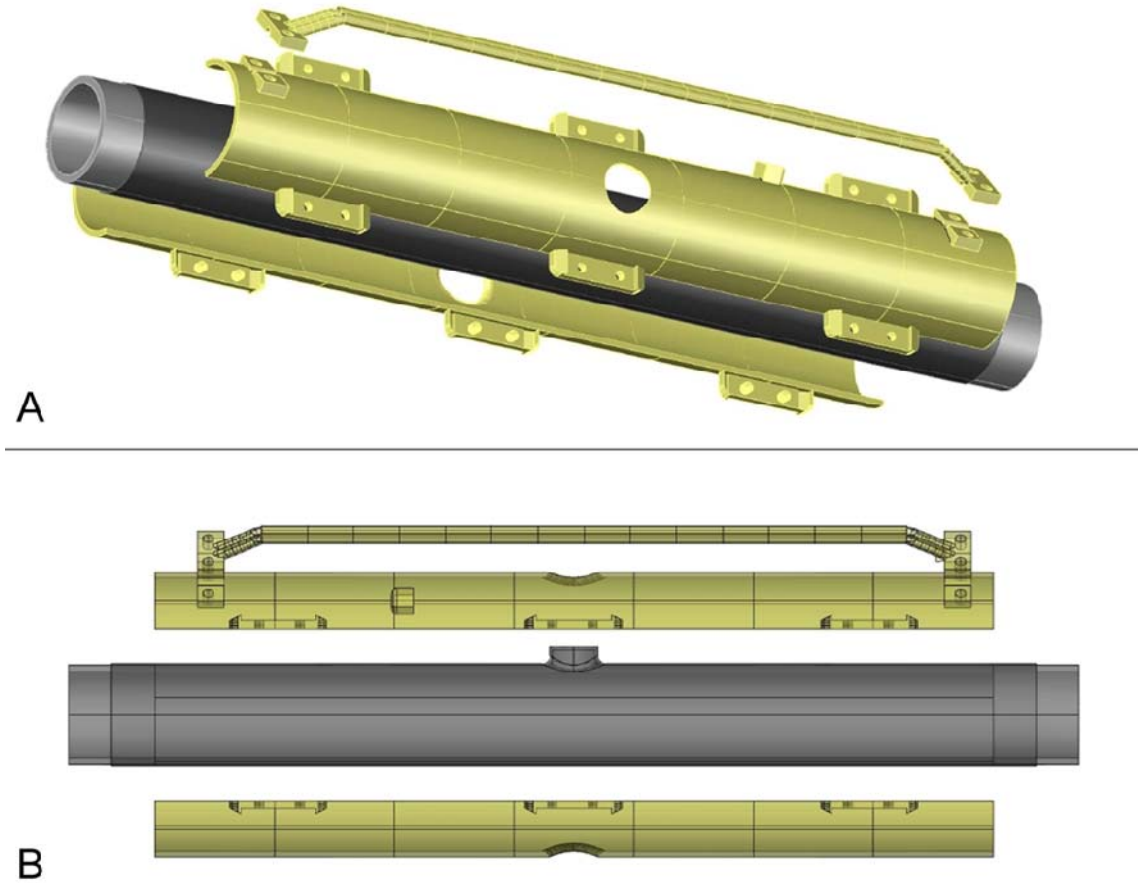

Figure 15: Proposed electrode design to prevent the electrode from moving upon well completion and keeping the electrode completely isolated from the steel well casing: (A) isometric view and (B) side view of assembly.

The attachment point for the electrode is critical to protect the relatively delicate copper conductors from both physical damage and corrosion. It is important that all of the exposed metal surfaces are created from the same type of metal (type 316 stainless steel). Figure 16 shows a possible takeout. The connection to the copper cable is encapsulated in polymer resin and brazed into the end of a piece of encapsulated stainless steel tube. The tubing acts as the final conductor and is attached to the electrode via standard, high pressure threaded couplings.

Two additional factors to be considered in the higher current EM source electrodes are the overall contact resistance of the electrodes and the ohmic heating of the

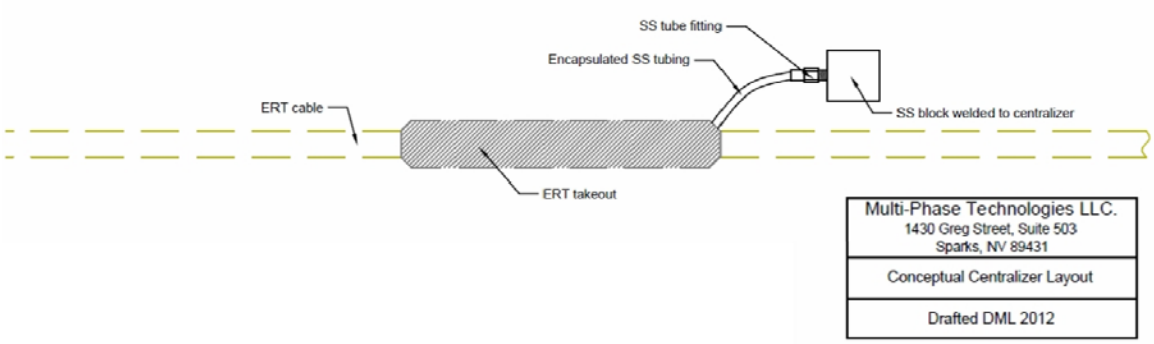

Figure 16: Drawing of a possible take out to prevent leakage along the casing.

electrodes. Virtually all of the electrical energy transmitted into the ground will be converted into heat. The fraction of the total energy dissipated near the electrodes is of particular concern. In Appendix A, the approximate heat generated by the electric current flow near the electrodes is derived. The increase in heat for a continuous current flow can be summarized as:

$$\Delta T \approx \rho I^2 A/k \tag{5}$$

The constant A is dependent only on the geometry of the electrodes, and k is the thermal conductivity of the formation. The thermal conductivity, k, depends on rock type and formation age, and is less variable than electrical resistivity. For a nominal thermal conductivity value of 3 (W/m/C), a casing diameter of 4.5 inches and lengths of 1, 2 and 3 meters, the value of A/k is approximately equal to 0.020, 0.086 and 0.0050 (C/VA/m), respectively. Table 2 shows the median values of resistivity near the Precambrian base rock of four well logs near the Aquistore site bedrock (White, 2012). For a resistivity value of 3 ohm-m, which corresponds to the median value above the Precambrian in Well *12106200613W200*, a current flow of 20 amps would generate temperature changes of 24°C for the shortest (1 m) electrode. The increase in temperature is likely to damage the insulation on the cables. Increasing the length of the electrode to 3 m would drop this value to about 6°C, which would be considered acceptable. For a background value of 21 ohm-m, the same 3 m electrode with a current of 20 amps would produce a temperature increase of 42°C, which could damage the insulation on the cables. In this case, the current flow would need to be reduced to below 10 amps to keep the temperature increase below 10°C.

Due to the high resistivity values, there is a high likelihood that the current flow within the Precambrian will be less than 10 amperes and possibly small fractions of an ampere. Due to the uncertainty in the resistivity near the Precambrian, it is important to place at least 3 source electrodes with two of the electrodes above the Precambrian interface. Although the configuration is less sensitive to the CO_2 plume in the reservoir, it is far more likely to produce sufficient current flow. It is important that the source electrodes be as long as possible. Unfortunately, the need

to keep the electrodes away from the casing joints limits the length of the electrodes to something substantially less than 13 m, the nominal length of the joints. This, and the difficulties in handling extremely long electrodes, limits the length to 2 or 3 m.

Table 2. The average resistivity from well log data in four wells near the Aquistore site. The resistivity values are given near the Precambrian bedrock

Well UWI	Top Precambrian (MD)	Median Resistivity 100 m Above Precambrian (Ohm-m)	Median Resistivity Below Precambrian (Ohm-m)	Median Resistivity Bottom 10 m
101150700308W200	3169.08	21.0	26.5	568
12106200613W200	2905.52	3.0	23.4	149
101132400203W200	2961.08	4.2	1,630	1,940
33023001710000W	3589.01	14.5	4,510	21,300

The second factor closely related to heating is the contact resistance of the electrodes. Both the power and the voltage of the sources are limited; the resistance of the cables and electrodes may also limit the maximum current flow and need to be considered in the design. For a cylindrical electrode the approximate contact resistance can be found from the single driven rod formula of Tagg (1964). Tagg's approximation for a rod at the surface is based on image theory, but one can back out the whole-space formula as:

$$R \cong \frac{\rho}{2\pi l}\, ln\left(\frac{2L}{d}\right) \tag{6}$$

where R is the approximate resistance of a grounded cylindrical rod, ρ is the background resistivity, L is the length of the rod, and d is the diameter of the rod. For the 3 m long electrode and a background resistivity of 21 ohm-m the electrode contact resistance is still only 5.18 ohm. At these resistances, the voltage drop at 20 amperes would be 103.6 volts and the power loss about 2,072 watts. Both the voltage drop and power lows are substantially lower than the capabilities of the transmitters and are not limiting factors in the current flow, even when the effects of two electrodes are added together.

Cable Design

Since the depth of the site is over 3,300 m, designing a durable cable is a key obstacle. The present design is to have separate cables for the EM source cable and ERT receiver cable(s). As discussed in the modeling section, separate transmitting and receiving cables are required if measurements are made with the receiver and transmitter in the same hole. An early borehole-to-surface EM study called for a single pair of source electrodes placed below the reservoir (Smith and Beyer, 2011); however, for Aquistore, we feel that three electrodes are needed for the source: two

below and one above the reservoir. This gives flexibility for increasing the signal-to-noise ratio and still leaves a source in the event that an electrode is damaged. The cable can be designed for two likely possible construction scenarios: (1) a combination of standard wire line cable and custom cable or (2) a continuous custom cable.

Design 1

Design 1 would use 3,100 m of standard armored wire-line cable. The suggested cable is the Rochester Cable 12-H-464. This cable has 12 conductors of 20 gauge wire. This cable consists of 12 wires plus filler material wrapped with tape and covered with two layers of steel armor. This design would use identical 12 conductor cables for both EM and ERT. For ERT, each individual conductor would attach to a single electrode. Each wire will have about 120 ohms resistance.

The EM cable will use three conductors together to reduce the resistance to about 40 ohms. The remaining wires in the EM bundle will connect to three additional ERT/style electrodes to give a total of 15 ERT electrodes, plus three EM source electrodes. The transition at the bottom of the borehole will need to have a very high-strength clamp design to pick up the force on the cable. The cable will need to be clamped periodically along the length of the casing.

The advantages of the armored wire-line cable are:

Durability: the steel armor is designed for deep borehole use and has a high probability of surviving to the required depth.

Shielding: for the EM technique the armor would act as a cable shield, giving some electrical separation between the transmitter and receiver bundles. Without the shield, it is not possible to conduct single-well EM.

Price: If the lowest temperature range (135°C continuous) is used, the cable is about $2.25 per foot (0.3048 m). This puts the cost of the cable at about $25,000 per cable, (which is lower than initially estimated as part of the Aquistore planning). The next highest temperature range cable increases the price to $3.25 per foot (0.3048 m) or about $35,000. (Note that this does not include the bottom 200 m of cable, electrodes, fabrication, and clamps, which could be substantial costs). Table 3 provides the estimated costs for the armored wire line cable.

Testing: Since this is a stock cable, samples could be received quickly for clamp designs, connection tests, etc.

Scheduling: The ERT arrays can be built in parallel with the cable manufacture and spliced on at the end. Although a special cable run is needed, it would be a short run. Most of the companies that build out small-run custom cables are not equipped to handle 3,400 m runs of cable.

Redundancy: We would have two cables with somewhat overlapping capabilities; as with any deep installation, there is a chance of failure, and having two cables makes it likely that at least some functionality would be present.

The disadvantages are:

Transition: We will need a transition/splice at ~3,100 m to a custom cable type, because the armored cable will short circuit the ERT electrodes. Stripping the armor away for the bottom 200 m is not an option either, because of the way the cable is designed. If the armor were stripped, then the remaining loose wire would never survive. The transition is a major reliability issue and was likely the source of problems at the Cranfield site (La Brecque, pers. comm, 2012). Since there will be a transition from high tensile strength cable (18,000 lbf) to low tensile strength (probably 1,000 to 2,000 lbf), there will need to be a clamp system that can pick up the difference, so that any tension on the upper 10,000 ft (3,048 m) of the cable doesn't tear the ERT section apart. At Cranfield, the clamps were pre-welded to the casing. The pre-welded clamps created several issues. First, they had to do the splice on the rig floor. Since the cables had to be trimmed to the correct length, this meant they could not "pot up" the splice, and it apparently leaked water over time. Also, one of the transitions became damaged in handling of the casing; the order of the wires were mixed up during the splice process.

Bottom Cable: We need a run of custom cable to build out the electrode arrays. The manufacture time may be as long as fabricating the main cables.

Electrical Leakage: The armor is a potential electrical leakage path. If there is a pinhole anywhere in the 11,000 ft. (3,353 m) of cable, water will go into the cable (water in the cable is inevitable over time) and will create a leakage path from the wire to the armor. We will have the company add a silicon water block to the cable to help reduce this risk; however there is a fairly good chance of one or more conductors having leaks over long time periods.

Table 3. Estimated Costs for the armored wire line cable (Design 1)

Item	**Est. Cost**
Armored ERT cables	$71,500
Armored Source Cables	$34,375
Polymer ERT Cables	$8,550
Polymer Source Cable	$4,275
Transition	$15,000
Fabricating Cable Takeouts	$9,000
Electrodes	$18,000
Total	**$160,700**

Design 2

Design 2 would use custom cable for both the ERT sensor electrodes and EM source electrodes. Design 2 would use custom-built metal-tubing encapsulated wires. A total of three encapsulated tubes would be included: two ¼-inch tubes each containing seven 20 gauge conductors, and one 5/16-inch tube containing three 14 gauge conductors. To allow connection to the electrodes, the "cables" would be custom-manufactured without the metal tubing, but with polymer encapsulation on the bottom 200 m of the cables.

The advantages of this design are:

Robustness: Using tubing-encapsulated cable is the most robust method of building the cable and has a high likelihood of surviving to depth.

Electrical Isolation: This would likely be a better cable with a greatly reduced chance of leakage over Design 1. This is likely the most important consideration, since the underlying reason for the cable is to collect good electrical data.

Source wire resistance: With the custom cable, we can get the single source wire resistance lower than the armored cable, down to about 30 ohms. Unfortunately, this wire resistance is too high to achieve a current flow of 20 amps with any of the transmitters listed in Table 1. The total wire resistance for both electrodes in a transmitting dipole would be 60 ohm. At 20 amperes, this would result in a voltage drop of 1,200 volts, too large for the Phoenix or Zonge transmitters, and a power loss of 24,000 watts, too large for the Iris transmitter. However, if the formation resistance is low enough, it should be possible to achieve current flows of 15 amps.

Transition: The design of the transition would be essentially eliminated. Although the cable costs are substantially higher than the standard cables, much of this cost would be offset by reducing the need for highly specialized clamps along the casing. Table 4 shows the estimated costs for the custom-built cable.

The disadvantages of this cable design are:

Cost: The initial cost of this cable is significantly higher than the standard logging cable.

Testing: No samples are likely available; some of design may have to wait for the cable to be complete.

Time: Delivery times are likely to be longer for the custom cable.

The bulk of the costs listed in Tables 3 and 4 for both designs are the cost of the cables themselves. Not included in the costs are the insulating coating, modification of the cables, cables protectors, clamps, and clamp blocks. Cable costs for Design 1 are cheaper than those for Design 2. However, Design 2 offers a more robust design and will not need as robust of a clamping system as Design 1. Design 1 requires robust custom-designed clamps to maintain tension on the cables throughout the installation, whereas Design 2 could simply use industry-standard Cannon type clamps along the upper portions of the casing.

Table 4. Estimated Costs for the custom built cable (Design 2)

Item	**Est. Cost**
ERT cables	$134,420
Source Cables	$66,660
Misc.	$3,444
Fabricating Cable Takeouts	$9,000
Electrodes	$18,000
Total	**$231,524**

Engineering Design Conclusions/ Recommendations

Although the primary costs for the cables and electrodes are higher for Design 2, the overall, installed cost of both designs are going to be nearly equivalent. Design 2 is less dependent on rigorous clamping of the cable, which will be an extra expense. In addition, Design 2 is superior both mechanically and electrically. Unfortunately, a number of costs could not be fully evaluated at the time of design, since they require a more complete design of the well, more communication with groups involved in designing and completing casing, and those deploying other instrumentation on the casing. Both of the proposed designs would require insulating not only the casing, but the tubing or cables running to other instruments in the deployment zone. Also, both designs will require modification to the casing to allow robust clamping of the electrodes and cables to the casing. The proposed clamping solutions incorporate welding blocks to the casing, then covering them with fiberglass insulation. This will require either a long lead time or performing fabrication on the well site. One additional advantage to Design 2 is that it is possible, with careful design, to construct a clamping system for the electrodes that would not require the welding of blocks to the casing. A similar system was deployed in the injection well at Ketzin (C. Schmidt-Hattenberger, pers. comm, 2012). Although that deployment was a shallow site, the proposed electrodes are much longer, more robust, and could be designed with much higher clamping force achieving static friction forces approaching the tensile failure forces of the casing.

Appendix A Cable Heating

Nearly all of the electrical energy transmitted into the borehole will be converted to heat in the cables, electrodes, and the formation. Although the overall energy loss in the cable can be quite large, the heat will dissipate over a very large volume and will not cause a significant temperature rise in the cable itself. However, on and near the electrodes, energy is dissipated over a fairly small area, possibly increasing the temperature to the point of damaging the cable or the electrical coating on the cables. This increase in temperature is discussed below.

For a given current flow, formula for electrical contact resistance (Equation a1) can be used to estimate the total steady-state heat dissipation within the formation as

$$WT = I^2 \cdot R \tag{a1}$$

where WT is the total dissipated power, I is the current flow, and R is the electrode contact resistance.

The temperature increase near an electrode.

To calculate the temperature increase near the electrode, we assume both the current flow and heat flow to be radially outward. This should be a good approximation near the center of the electrode for radial distance much less than the length of the electrode.

The volumetric Joule heat flow is given by:

$$q = e \cdot j = |j|^2 \rho \tag{a2}$$

where q is heat flow, ρ is the background resistivity, e is the electric field and j is current density. For the case where the current flow is radially outward from a circular rod, the current density, j, at radius r, is given by:

$$j = \frac{I}{L}\frac{1}{2\,\pi r} \tag{a3}$$

where L is the length of the rod. So total dissipated heat between the surface of the rod, r_1, and some radius r_2 would be:

$$q = \int_0^L \int_0^{2\pi} \int_{r1}^{r2} \rho \left(\frac{I}{L}\frac{1}{2\,\pi r}\right)^2 r\partial r\partial\theta\partial z = \frac{\rho I^2}{2\pi L}\ln\left(\frac{r2}{r1}\right) \tag{a4}$$

If the heat flow, q, were entirely dissipated on the casing surface, radius r_1, then the temperature increase, ΔT, for the same volume would be given by:

$$\Delta T = \frac{q_1}{2\pi Lk} \ln\left(\frac{r2}{r1}\right) \tag{a5}$$

where k is the thermal conductivity and q_1 is the heat dissipated at radius r_1.

Simply combining Equations a4 and a5 overestimates the ΔT, since the heat is dissipated throughout the volume. The incremental heat flow in the region r_1 to r_2 near the electrode can be found by substituting r for r_1 and taking the derivative of the Equation (a4) with respect to r:

$$q'(r) = \frac{\rho I^2}{2\pi L}\left(\frac{1}{r}\right) \tag{a6}$$

Combining equations a5, a6, and integrating gives:

$$\Delta T = \int_{r1}^{r2} \frac{\rho I^2}{2\pi L}\left(\frac{1}{r}\right)\frac{1}{2\pi Lk}\ln\left(\frac{r2}{r}\right)\partial r = \frac{\rho I^2}{8\pi^2 L^2 k}\left(\ln\left(\frac{r2}{r1}\right)\right)^2 \tag{a7}$$

This formula is only valid near the electrode, where the electric current flow pattern and density is similar to that of a two-dimensional rod. The approximation breaks down for a radius greater than about ½ L. Substituting r_2 = ½ L gives the final equation:

$$\Delta T \approx \frac{\rho I^2}{8\pi^2 L^2 k}\left(\ln\left(\frac{0.5\,L}{r1}\right)\right)^2 \tag{a8}$$

Acknowledgements

This work was supported by the CO_2 Capture Project (CCP). We acknowledge the support of the Aquistore Project, operated by the Petroleum Technology Research Center. We thank K. Dodds of the CCP for support and technical discussion of this work. G.M. Hoversten provided logs for Imperial Halkett Well 15 7 3 8. W. Zaluski provided additional neighboring logs. We thank D. White for project technical support.

Lawrence Berkeley National Laboratory is supported by the U.S. Department of Energy under Contract No. DE-AC02-05CH11231.

References

Andreis, D. L., & MacGregor, L. M. (2010). Using CSEM to Monitor the Production of a Complex 3D Gas Reservoir - A Synthetic Case Study. *EAGE*, June 2010, 14 - 17.

Commer, M. and Newman G. A., 2008, New advances in controlled source electromagnetic inversion: Geophysical Journal International, 172, 513-535.

Doughty, C., 2009. Investigation of CO_2 plume behavior for a large-scale pilot test of geologic carbon storage in a saline formation, Transport in Porous Media, special issue on geologic carbon storage, doi:10.1007/S112423-009-9396-z.

Hoversten, G,.M., and E. Gasperikova, E., 2006. Investigation of novel geophysical techniques for monitoring CO_2 movement during sequestration. Report to Carbon Capture Project, Lawrence Berkeley National Laboratory, publication no. 56822.

LaBrecque, Pers comm. (2012)

Ministry of Environment, 2012, Go green Saskatchewan: Aquistore, http://www.environment.gov.sk.ca/adx/aspx/adxGetMedia.aspx?DocID=2c5457f7-e395-4812-a465-4aee70ec6e11&MediaID=1519&Filename=AQUISTORE+fact+sheet.pdf&l=English

Press, W.H., Flannery, B.P., Teukolosky, S. A., and Vetterling, W.T., Numerical Recipes, The Art of Scientific Computing, Cambridge Univ. Press, Cambridge, Great Britain, 1986, pp 472-473.

Petiau, G. and Dupis, 1980. A. Noise, temperature coefficient, and long time stability of electrodes for telluric observations, Geophys. Prosp. 28 (5), 792-804.

Petroleum Technology Research Center (PTRC), 2011, Aquistore: Saskatchewan's deep saline CO_2 storage research project, http://www.environment.gov.sk.ca/adx/aspx/adxgetmedia.aspx?MediaID=001689ad-a72e-4a96-b99b-cf45cf01b7db&Filename=Aquistore%20Fact%20Sheet%202012.pdf

Schmidt-Hattenberger, C., personal conversation, 2012.

Schmidt-Hattenberger, Cornlia, Peter Bergmann, Dana Kielbling, Kay Kruger, Carsten Rucker, Hartmut Schutt, Ketzin Group, 2011, Application of a vertical electrical resistivity array (VERA) for monitoring CO_2 migration at the Ketzin site: First performance evaluation, Energy Procedia, **4**, 3363-3370.

Smith, J. T.,and Beyer., J.H., 2011, Monitoring CO_2 Sequestration using a down-well electric dipole and surface receivers, LBNL, Unpublished manuscript.

Swanepoel, R., Harris, B. and Pethick, A. 2012. Three dimensional modeling for time-lapse cross-well CSEM monitoring of CO_2 injection into brine filled reservoirs. Eleventh meeting of the Australian Society for Exploration Geophysics (Abstract).

Tagg, G. F., 1964, Earth Resistances, London Newness

Tøndel, Richard, Jon Ingham, Douglas LaBrecque, Hartmut Schütt, David McCormick, Robert Godfrey, Jose A. Rivero, Scott Dingwall, and Andrew Williams, 2011, Reservoir monitoring in oil sands: Developing a permanent cross-well system: Society of Exploration Geophysicists, Expanded Abstracts, **30** (1), 4077-4081.

White, D., personal conversation, June 14, 2012.

Whittacker, S., Worth, K., Preston, C., 2009. Aquistore: CO_2 storage in deep brines in Saskatchewan Canada. Presentation at Institut Francaise Petrolier, Rueil-Malmaison, France, May 2009 (as at http://www.ifpenergiesnouvelles.com/content/download/67983/1473837/file/26_Whittaker.pdf, accessed March 2012).

DISCLAIMER

This document was prepared as an account of work sponsored by the United States Government. While this document is believed to contain correct information, neither the United States Government nor any agency thereof, nor The Regents of the University of California, nor any of their employees, makes any warranty, express or implied, or assumes any legal responsibility for the accuracy, completeness, or usefulness of any information, apparatus, product, or process disclosed, or represents that its use would not infringe privately owned rights. Reference herein to any specific commercial product, process, or service by its trade name, trademark, manufacturer, or otherwise, does not necessarily constitute or imply its endorsement, recommendation, or favoring by the United States Government or any agency thereof, or The Regents of the University of California. The views and opinions of authors expressed herein do not necessarily state or reflect those of the United States Government or any agency thereof or The Regents of the University of California.

Ernest Orlando Lawrence Berkeley National Laboratory is an equal opportunity employer.